Monitoring of in-vitro ultrasonic stimulation of cells by numerical modeling

M. Majnooni, P. Lasaygues, V. Long, J.-C. Scimeca, D. Momier, F. Rico, N. Buzhinsky, C. Guivier-Curien, C. Baron

Monitoring of in-vitro ultrasonic stimulation of cells by numerical modeling

M. Majnooni[a,b,*], P. Lasaygues[c], V. Long[c], J-C. Scimeca[d], D. Momier[d], F. Rico[e], N. Buzhinsky[e], C. Guivier-Curien[b], C. Baron[a]

[a] *Aix Marseille Univ, CNRS, ISM UMR 7287, Marseille, France*
[b] *Aix Marseille Univ, CNRS, Centrale Marseille, IRPHE UMR 7342, Marseille, France*
[c] *Aix Marseille Univ, CNRS, Centrale Marseille, LMA UMR 7031, Marseille, France*
[d] *Université Côte d'Azur, CNRS, Inserm, iBV, France*
[e] *Aix Marseille Univ, INSERM UMRS 1067, CNRS UMR 7333, LAI, Marseille, France*

Abstract

Ultrasound stimulation of living tissues is a promising technique that can be safely applied for regenerative treatments. However, the ultrasound-induced mechanotransduction is still not well understood because of the large number of parameters involved at different scales and their difficult experimental accessibility. In this context, in-vitro studies may help to gain insight into the interaction between ultrasound and cells. Nevertheless, to conduct a reliable analysis of ultrasound effects on cell culture, the monitoring of the acoustic intensity delivered to the cells is of prime interest. Thanks to the development of an innovative custom experimental set-up inspired from ultrasound stimulation of bone regeneration conditions, major disturbing phenomena such as multiple reflections and standing wave formation inside the Petri dish are eliminated. Thus, the level of ultrasound stimulation, especially, in terms of spatial average and temporal average intensity (I_{SATA}), delivered to the cells can be monitored. Then to properly estimate the level of ultrasound stimulation, a finite element model representing the experimental in-vitro configuration is developed. The numerical model manages in capturing the characteristics of the experimentally measured acoustic intensity distribution as illustrated by the experimental and

*Corresponding author
Email address: meysam.majnooni@univ-amu.fr (M. Majnooni)

numerical I_{SATA} values of 42.3 and 45.8 mW/cm^2 respectively, i.e. a relative difference of 8%. The numerical model would therefore allow exploring data inaccessible to experimental measurement and parametric studies to be carried out and facilitates the investigation of different virtual experimental configurations.

Keywords: in-vitro ultrasound stimulation, acoustic intensity, numerical modeling

1. Introduction

Within the last three decades, many researchers focused on ultrasound (US) stimulation of living tissues and cells clinically and in animal and in-vitro models, confirming promising results [1–7]. Thus, these experimental works and clinical studies demonstrated that low intensity pulsed ultrasound (LIPUS) induced mechanical effects liable to trigger bone remodeling. However, the underlying mechanisms of this ultrasonic cell mechanotransduction are still unclear and bone regeneration (USBR) remains controversial [8–12].

In order to address this issue and lay the groundwork for understanding the ultrasonic cell mechanotransduction, in-vitro studies on cells are an essential step.

Different approaches in in-vitro US stimulation are reported in literature but several of them stress the difficulty of controlling disturbing phenomena and monitoring the level of US stimulation. Indeed, in the most common configuration called "well on water surface" configuration [13], a major concern is the reflection of the incident wave at the interface between cell culture medium and air. In this case, the reflected wave interacts with the incident wave and can generate uncontrolled interferences such as standing waves that prevent an accurate prediction of US stimulation level. These disturbing interferences strongly depend on the growth medium height [13–15]. For instance, Hensel et al. [13] reported a variation of $\lambda/4 \approx 0.5$ mm in growth medium height can lead to the increase or decrease of the acoustic pressure amplitude by the factor

of 2 inside the Petri dish. In the "well on water surface" configuration, the level of the acoustic exposure inside the Petri dish is also dependent on the distance between the US emitter and the Petri dish bottom. It has been reported by several experimental and numerical studies [16–18], but this value varies greatly from one study to another.

Highlighted by these studies and others [19, 20], special attention must be paid to distances and dimensions of the experimental set-up which significantly influences the US exposure conditions and monitoring inside the Petri dish.

Aware of the importance of controlling the conditions of US stimulation to achieve a relevant interpretation of the results, some studies propose a characterisation of the acoustic field delivered in the Petri dish. However, to the authors' knowledge, none of them propose a method for predicting and monitoring the level of in vitro US stimulation.

Inspired by common experimental set-ups [16, 21–23] and performed numerical analyses [17, 18], the present study uses an experimental set-up including an innovative absorbing system to prevent multiple reflections and standing wave formation, thus allowing the monitoring of the ultrasonic stimulation level of the cells when they will be seeded inside a Petri dish.

From these controlled US stimulation conditions, a numerical model based on the experimental set-up is developed in COMSOL Multiphysics® in order to assess a quantitative estimation of the acoustic intensity (level and distribution) where the cells are supposed to be seeded. This first model will be one of the tools to understand cell mechanotransduction induced by US. The comparison of experimental and numerical estimations of the acoustic intensity (level and distribution) is used to tune and validate the numerical model. Once validated, the numerical model allows the assessment of the US stimulation level at the dish surface where the cells would be located, and this measurement is not experimentally accessible. Moreover, parametric studies could be performed using the numerical model to investigate the effects of different geometries and acoustic signals to predict the US stimulation level and to guide the choice of the optimized in-vitro US stimulation. The novelty of this approach is the numerical

estimation of the acoustic intensity inside the Petri dish at the potential cell location under controlled in-vitro US stimulation conditions.

2. Materials & Method

2.1. Intensity definition

The increasing use of ultrasonic devices in medical applications makes it necessary to establish a standard procedure to measure the acoustic output of these devices and thus control the potentially induced biological effects. It is important to know the acoustic output not only should be able to calibrate the measurements, but also should to be capable to predict the field for various exposure conditions [24].

In designing and development of US medical applications, acoustic intensity which is defined as the rate of energy transfer per unit time per unit area, is a key parameter. The temporal average intensity (I_{TA}) for a pulsed wave is then given by

$$I_{TA} = \frac{1}{T_{PRP}} \int_0^{T_{PRP}} \frac{p^2(t)}{\rho c}\, dt \tag{1}$$

where p(t), ρ, c and T_{PRP} are the acoustic pressure, the density, the speed of the sound in the medium, and the pulse repetition period respectively. In most para/medical devices, more descriptive criteria like I_{SATA} are required, which is the I_{TA} averaged over the beam cross-sectional area. The most widely used definition of the I_{SATA} is the one given by the FDA as

$$I_{SATA} = \frac{1}{A_6} \iint_{A_6} I_{TA}\, ds \tag{2}$$

where A_6 is -6 dB beam cross-sectional area such that the I_{TA} measured at a point inside A_6 is greater than 25% of the spatial peak temporal average intensity I_{SPTA} [25]. A simple method to calculate the I_{SATA} is proposed by Preston [26]

$$I_{SATA} = \frac{1}{N}\sum_{i=1}^{N}(I_{TA})_i\,, \quad (I_{TA})_i \geq 0.25 \times I_{SPTA} \tag{3}$$

where N is the total number of points measured inside the beam cross-sectional area.

2.2. Experimental set-up and workflow

Transducer, hydrophone, and the water bath. The experiments are carried out with an immersion transducer (Imasonic, Voray-sur-l'Ognon, France) with a center frequency of 1 MHz. The active diameter of the transducer is 13 mm. In transmission mode configuration, acoustical measurements are performed using a needle hydrophone with 0.5 mm diameter, a submersible wide-band amplifier and a converter-coupler (Precision Acoustics Ltd, Dorchester, UK). The sensitivity of the needle hydrophone at 1 MHz is 426 mV/MPa according to the technical data sheet provided by the manufacturer. The transducer and the placed overlying hydrophone are immersed in a degassed-water tank. The velocity of the ultrasonic wave in water is equal 1474 m/s for a water bath temperature of 17.8°C. The experiment room is air-conditioned and is kept at a constant temperature. Experimental conditions do not change during the tests.

Characterization of the acoustic field. The first step is to characterize the acoustic field of the transducer. To do so, the transducer is driven by a waveform generator (TGA 1241, Thurlby Thandar Instruments Limited, UK). The distance D (from the transducer to the water/air interface) and the distance z (from the transducer to the hydrophone) (Fig. 1) are first controlled using an ultrasonic pulse-mode method, in reflection mode (the distance D), or transmission mode (the distance z).

In the case of pulse-mode method, the temporal source waveform is a signal comparable to a Dirac delta function (in terms of the distribution), and the output signal delivered by the transducer is comparable to a broadband Gaussian function with a time duration of 6 μs. The radio-frequency signals

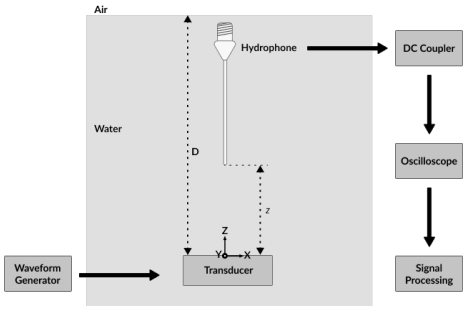

Figure 1: Synoptic view of the data acquisition and relative positioning of the hydrophone and transducer ($D = 450$ mm and $z \in [3, 48]$ mm)

.

(RF-signals) are conveyed from a 12-bit oscilloscope (Lecroy HDO 6104, Teledyne Inc., Thousand Oaks, USA) to a personal computer using a USB interface file transfer, and stored. The signal processing algorithms are implemented using MATLAB® (The MathWorks, Inc., Natick, Massachusetts, USA).

To scan the US field, a micrometric electro-mechanical positioning scanner is used to position the hydrophone, related to the active surface of the transducer, and to evaluate the wave fields in the different XY planes along the Z-axis. The distance traveled along the Z-axis is 45 mm, from 3 mm to 48 mm, with a linear increment of 1 mm. Along the X and Y axes, the distance traveled is 15 mm with a linear increment of 0.5 mm. For each position, an acoustic signal is recorded, and the peak acoustic pressure is estimated from the measurement (Volts versus sensibility of the hydrophone) of the maximum of the Hilbert transform modulus of the RF-signals. Fig. 2a shows the normalized peak acoustic pressure in both planes. The ultrasonic pressure distribution along Z-axis is then obtained from the peak pressure measured at the center along the Z-axis perpendicular to the surface of the transducer (Fig. 2b). As expected, three zones can be distinguished: the near field from 3 mm to 25 mm where the increasing peak acoustic pressure is unstable, the Fresnel zone between 25 mm and 38 mm where the trend is more stable, and the far field after 38 mm where the peak acoustic pressure decreases.

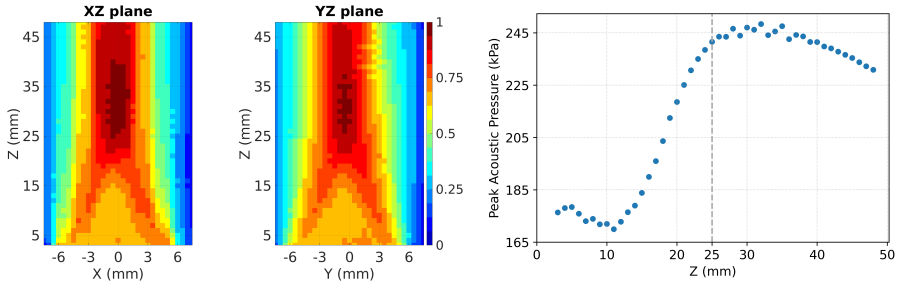

(a) (b)

Figure 2: (a) Normalized peak acoustic pressure in XZ and YZ planes, (b) US pressure distribution along the Z-axis of the transducer.

Petri dish location. The Petri dish used in these experiments is a Corning model (ref. 430196) with an external diameter of 55 mm, a depth of 15 mm and a wall and bottom thickness of 0.8 mm. The material constituting the Petri dish is polystyrene, in which the measured ultrasonic wave velocity equals 2367 m/s, which is in accordance with the literature [27]. It is necessary to mention that for the study presented here, no biological cells were introduced into the Petri dish. The Petri dish is held above the transducer with a support that does not disturb the performance and the acoustic field of the transducer. The distance h in Fig. 3 between the transducer and the Petri dish (controlled using the ultrasonic pulse-mode method, in reflection mode) is set to 25 mm (*i.e.* the beginning of the Fresnel zone) to ensure maximum energy transmission and stability in the Petri dish (Fig. 2b).

Absorbing system. A custom-designed absorbing system developed in the lab is mounted above the Petri dish as shown in Fig. 3c. The dimensions, assembly and materials have been carefully thought out and chosen to be compatible with cell culture. A quick presentation is given in the following paragraphs.

The developed absorbing system was validated comparing three configurations designed as discussed below:

- HW: High water level without absorbing system (Fig. 3a);

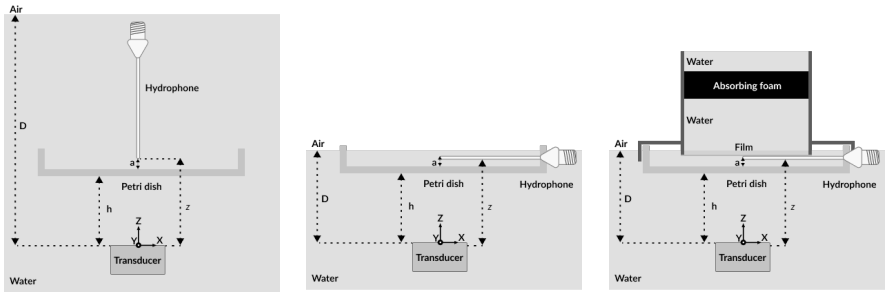

(a) (b) (c)

Figure 3: Three configurations: (a) HW: High water level without absorbing system, (b) LW_{Off}: Low water level without absorbing system, (c) LW_{On}: Low water level with absorbing system. In all the three configurations, the distances $h = 25$ mm and $z = 28$ mm.

- LW_{Off}: Low water level without absorbing system (Fig. 3b);
- LW_{On}: Low water level with absorbing system (Fig. 3c).

For all experiments presented from now on, the temporal source waveform is a 1 MHz-burst signal with a duration of 200 μs, an amplitude of $10V_{pp}$ (50 Ω), and a pulse repetition period (T_{PRP}) equal to 1 ms. It is also useful to note that the configuration LW_{Off} is similar to the "well on water surface" configuration studied by Hensel et al. [13] which is one of the classical ways to investigate the in-vitro US stimulation of cells.

In the three configurations, the tip of the hydrophone was placed right in the center of the Petri dish at the distance $a = 2.2 \pm 0.1$ mm from the bottom of the Petri dish corresponding to $z = 28$ mm, and the distance D (transducer-water/air interface) (Fig. 3) was sufficient to ensure that the hydrophone tip remained fully immersed in vertical or horizontal positions. It is helpful to mention that the distance D (equal to 450 mm) in Fig. 3a was much larger than the distance z in order to prevent any interference with reflected waves at the water/air interface in HW configuration. The time evolution of the sound pressure at this point was compared for each of the 3 configurations (Fig. 4).

Comparative analysis over a duty cycle indicated that the relative mean differences between HW and LW_{Off} configurations and between LW_{On} and LW_{Off}

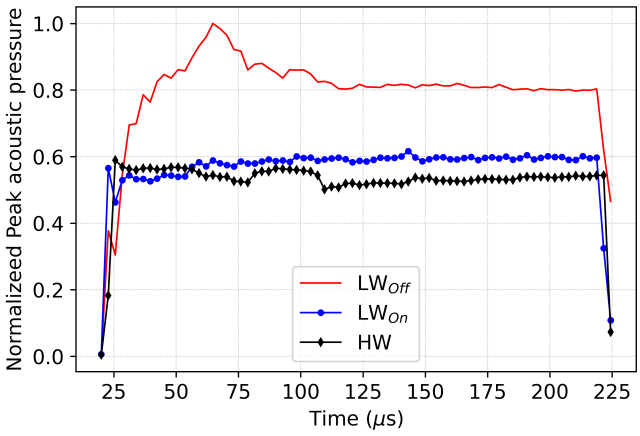

Figure 4: Modulus of the Hilbert transform of the transmitted RF-signals at the distance $z = 28$ mm along the axis of the transducer

.

were 52% and 41% respectively while it was only about 8% between $\mathrm{LW_{On}}$ and HW. This confirms that the innovative absorbing system met its stated objective by providing equivalent behaviour as high amount of water meaning negligible perturbing phenomena. This equivalency between HW and $\mathrm{LW_{On}}$ configurations provides the opportunity to perform current study in the HW configuration and then apply the findings to future biological experiments with the $\mathrm{LW_{On}}$ configuration.

2.3. Numerical Model

In this study, a numerical finite element model is developed in order to assess the level and distribution of the acoustic intensity delivered at the location where the cells would be seeded, a location corresponding to a few microns above the dish bottom surface, inaccessible experimentally with a hydrophone.

Inspired by the HW configuration (Fig. 3a), the numerical model is implemented using the Pressure Acoustics, Transient module of the commercial software COMSOL Multiphysics® v5.4. Due to cylindrical nature of experimental set-up, the corresponding numerical model is considered to be 2D axi-symmetric.

All dimensions and US parameters such as frequency, pulse repetition frequency, and duty cycle, are those used in the experimental measurements. Modulus of the elasticity, density and Poisson's ratio of the polystyrene Petri dish are 3.6 GPa, 1050 kg/m^3, and 0.34 respectively. Density and sound speed of the water are 1000 kg/m^3 and 1474 m/s respectively.

To mimic HW configuration, perfectly matched layer (PML) condition is applied as boundary conditions on the water domain and on the top boundary of the culture medium. The transducer is modeled as a boundary condition generating an incident pressure wave defined as

$$\mathrm{p}(t,z) = \begin{cases} \mathrm{p}_0 \sin(2\pi f t - z/c_w) & 0 < t \leq 200\ \mu\mathrm{s} \\ 0 & 200\ \mu s < t \leq 1\ \mathrm{ms} \end{cases} \tag{4}$$

where $f = 1$ MHz, z and c_w are frequency, wave propagation direction and wave velocity in water respectively. p_0 is the incident pressure amplitude which will be determined later in Section 3.1.

An acoustic-structure boundary is applied on the water/polystyrene dish interfaces to couple pressure acoustics equations to solid mechanics equations requiring the continuity of the normal component of velocity and the balance of forces at the interfaces.

The maximum mesh size is set to $\lambda/10$ where λ is the acoustic wavelength in each medium. That is to say, the maximum element size in water and polystyrene Petri dish corresponds to 0.15 and 0.24 mm respectively. The complete mesh consists of 29324 quadrilateral elements.

A necessary condition for the stability of a numerical scheme is that the numerical domain of dependence bounds the physical domain of dependence which is met by satisfying the Courant-Friedrichs-Lewy (CFL) number [28]. In this study, time stepping is set to 40 ns to meet the CFL condition.

The computation time on a Dell® 7490 with 1.9 GHz processor and 16 MB RAM, running on Ubuntu 18.04 LTS operating system, was approximately 55 minutes.

2.4. Intensity calculations

The experimental pressure distribution is measured by scanning the XY-plane at the distance $z = 28$ mm, and the intensities I_{TA}, I_{SPTA}, and I_{SATA} are then calculated (Eqs. 1 and 3). The total scanned area is 2.25 cm^2 (15×15 mm^2) with a pitch of 0.25 mm. The intensities are calculated from stored RF-signals, following the procedure describes above. The numerical intensities, I_{TA}, I_{SPTA}, and I_{SATA}, are estimated from the acoustic pressure map calculated at the distance $z = 28$ mm.

3. Results

3.1. Experimental and numerical matching

A first reference measurement is made in water at the distance $z = 28$ mm to estimate the I_{TA} distribution (Fig. 5). The intensity I_{SPTA} is valued at 89.6 mW/cm^2 allowing to define the A_6 surface (Eq. 2) and calculate the intensity I_{SATA} applying Eq. 3.

As the exact incident pressure delivered at the transducer active surface is not experimentally accessible, a parametric study is carried out to define the incident pressure amplitude p_0 implemented in the numerical model (Eq. 4). Using the numerical model, the relationship between p_0 and I_{SPTA} and p_0 and I_{SATA} (at $z = 28$ mm) is investigated (Fig. 6). A third order polynomial function allows determining the value of p_0 corresponding to the experimental calculations of I_{SPTA} and I_{SATA}. A good compromise to match experimental intensity measurements is $p_0 = 57$ kPa giving $I_{SPTA} = 90$ mW/cm^2 and $I_{SATA} = 45.8$ mW/cm^2.

Fig. 7a plots a comparison between the experimental and numerical distribution with a similar grid resolution 61×61 with a 0.25 mm pitch. The experimental and numerical intensities I_{TA} profiles along diameter are plotted in Fig. 7b.

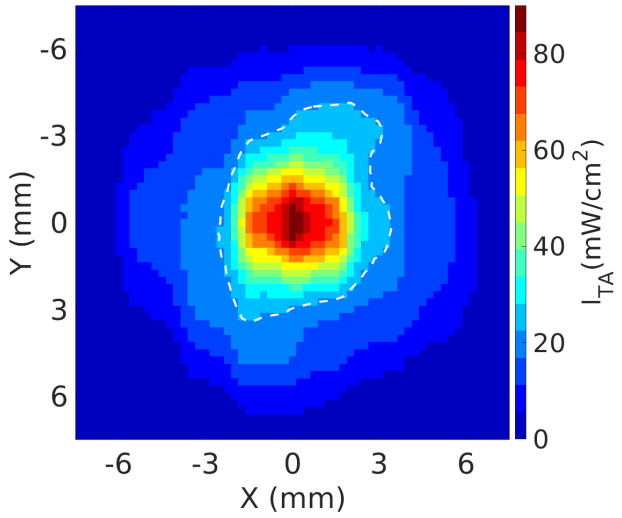

Figure 5: Experimental distribution of the intensities I_{TA} (averaged over 1ms-cycle of stimulation) at the distance $z = 28$ mm *without the Petri dish*. The white dashed contours indicate the $0.25 \times I_{SPTA}$ threshold that delineates the -6dB beam cross-sectional area (A_6). The corresponding intensity I_{SATA} is calculated inside this white dashed line.

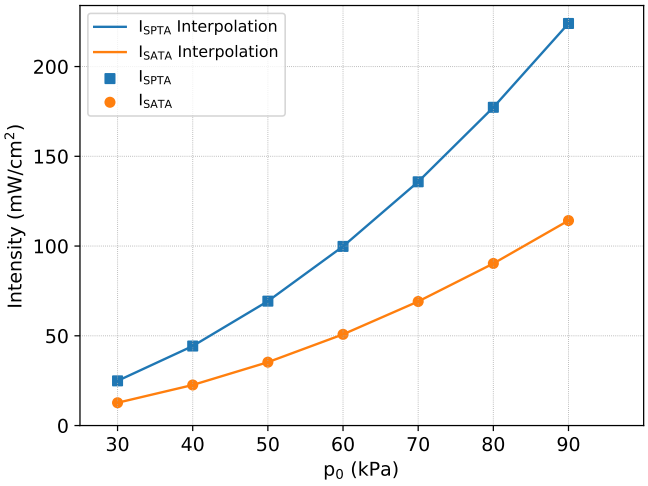

Figure 6: Values and interpolation of the intensities I_{SATA} and I_{SPTA} as function of the acoustic pressure p_0 estimated from the numerical model.

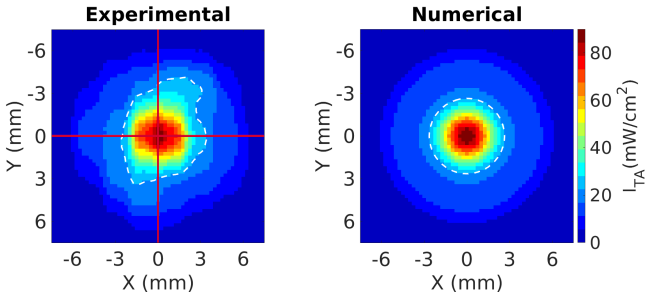

(a)

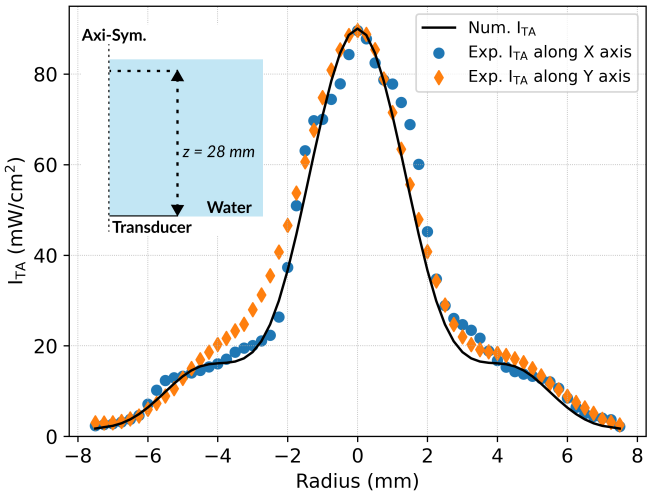

(b)

Figure 7: (a) Experimental and numerical I_{TA} estimation at the distance $z = 28$ mm in water *without the Petri dish*. The white dashed contours indicate the $0.25 \times I_{SPTA}$ threshold that delineates the −6dB beam cross-sectional area (A_6); (b) comparison of the experimental and numerical I_{TA} distribution. The experimental intensities I_{TA} are plotted along the red X (blue points) and Y (orange diamonds) axes.

Table 1: Experimental and numerical intensities I_{SPTA} and I_{SATA} [mW/cm^2].

	without the Petri dish		with the Petri dish	
	I_{SPTA}	I_{SATA}	I_{SPTA}	I_{SATA}
Experimental	89.6	42.3	81.4	38.4
Numerical	90	45.8	81.9	36.8
Difference	0.4%	8%	0.6%	4%

3.2. Inside the Petri dish

Fig. 8a illustrates a comparison between experimental and numerical I_{TA} distribution inside the Petri dish, keeping the acoustic pressure $p_0 = 57$ kPa. The experimental intensities I_{SPTA} and I_{SATA} are 81.4 and 38.4 mW/cm^2 respectively. Their corresponding numerical values are 81.9 and 36.8 mW/cm^2. Fig. 8b plots the experimental and numerical I_{TA} profiles along the diameter of the Petri dish. A summary of the results is given in Table 1.

3.3. Comparative analysis

In future biological experiments, the cells will be seeded inside the Petri dish and their typical diameters vary from 5 to 20 μm. It is very delicate, if not impossible, to evaluate this location corresponding to a few microns above the surface of the bottom of the Petri dish without damaging the hydrophone. Therefore, with the help of numerical modeling, it is possible to make measurements which are not attainable by the experimental methods. For instance, the intensities I_{SPTA} and I_{SATA} at the distance 10 μm from the inner surface of the bottom of the Petri dish ($z = 25.81$ mm corresponding to position of the cells in biological in-vitro experiments) are 64.6 and 28.2 mW/cm^2 respectively. Fig. 9 represents the equivalent intensity distribution delivered at the location where the cells will be.

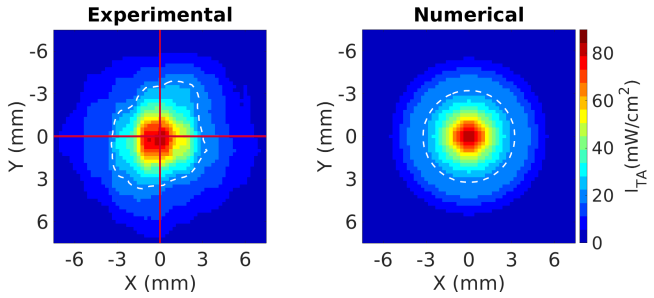

(a)

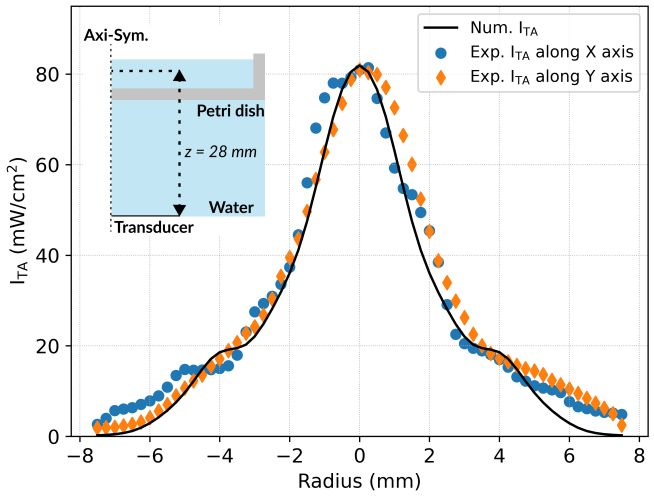

(b)

Figure 8: (a) Experimental an numerical I_{TA} estimation at the distance $z = 28$ mm in water *with the Petri dish*. The white dashed contours indicate the $0.25 \times I_{SPTA}$ threshold that delineates the −6dB beam cross-sectional area (A_6); (b) comparison of the experimental and numerical I_{TA} distribution. The experimental intensities I_{TA} are plotted along the red X (blue points) and Y (orange diamonds) axes.

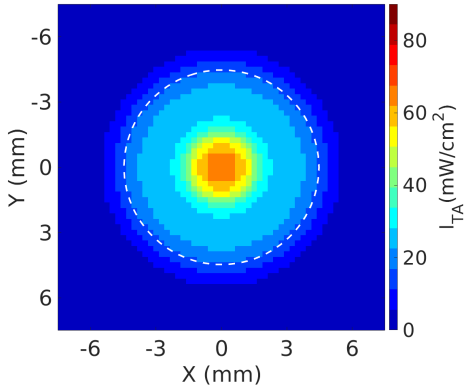

Figure 9: Numerical simulation of the I_{TA} distribution delivered to the hypothetical cells at the distance 10 μm above the Petri dish bottom. The white dashed contours indicate the $0.25 \times I_{SPTA}$ threshold that delineates the -6dB beam cross-sectional area (A_6).

4. Discussion

There are many studies in the literature dealing with in-vitro US stimulation, however the great variability of the stimulation parameters makes a comparative analysis of the published results difficult. A review by Padilla et al. [8] shows that for a given set of acoustical parameters, the configuration of the experimental set-up can lead to controversial results. For example, they cite that Unsworth et al. [29] applied 1.5 MHz US burst with 20% duty cycle at 1 kHz and the intensity $I_{SATA} = 31$ mW/cm^2 to pre-osteoblastic mouse cells and observed enhancement of matrix mineralization whereas Bandow et al. [30], using the same acoustic conditions, demonstrated no improvements. Further investigation reveled that, in Unsworth's experiments, the transducer was directly coupled to the bottom of the Petri dish whereas in Bandow's study, the exposure was far from the surface of the transducer with an absorbing chamber avoiding standing wave effects. These examples clearly state the importance of configuration set-ups and confirm the need for controlled conditions and monitorable system such as the one proposed in this study.

The goal of this study is to propose a numerical model allowing to estimate

and predict the level of US stimulation that will be delivered to the cells when they will be seeded in the in-vitro experimental set-up. This monitoring can only be assured under controlled conditions obtained thanks to the absorbing system.

Without the absorbing system, US waves are strongly reflected at the culture medium/air interface and have a strong effect on the acoustic pressure inside the Petri dish as shown in Fig. 4. This problem is frequently raised in the literature but rarely studied and resolved [13, 19, 23]. By mounting the absorbing system, US waves are fully transmitted to the absorbing foam (Fig. 3c) which isolates multiple reflections and avoid the formation of standing waves inside the Petri dish. Similar principles have been used in a few publications but without investigating their effectiveness [17, 21, 22]. The effectiveness of the developed absorbing system used in this study has been investigated (Fig. 4) demonstrating that the wave behaviour in the set-up with the absorbing system is similar to a high amount of water above the Petri dish.

Once the US stimulation conditions are under control, the milestone was to develop a numerical model that is essential to fully characterize the US field and estimate the value of the acoustic intensity potentially delivered to the cells inside a Petri dish. Furthermore, this numerical model will become a relevant tool to further investigate the different parameters affecting the acoustic intensity such as location of the Petri dish, frequency, and duty cycle.

As mentioned in the introduction, the issue is to monitor the level of US stimulation. This level is currently associated to the acoustic intensity and more precisely to the spatial average time average intensity I_{SATA} and the spatial peak time average intensity I_{SPTA}. From the finite-element model mimicking the experimental set-up, a relation between the source acoustic pressure p_0 and the I_{SATA} and I_{SPTA} estimated without the dish has been established (Fig. 6) in order to ensure similar US stimulation conditions between numerical and experimental models allowing them to be compared in a coherent way. Numerical and experimental I_{TA} maps calculated without the Petri dish are in accordance as shown in Fig. 7. The comparison of the intensity values but also of the I_{TA}

distribution is still satisfying when the Petri dish is placed above the transducer (Fig. 8). Table 1 summarizes that the numerical model captures the main trends of the experimental measurements in terms of intensity values I_{SATA} and I_{SPTA}. Once the relevance of the numerical model is established, it is possible to use it to evaluate the level of stimulation applied to the cell seeding area, which is not experimentally accessible (Fig. 9).

The current study was subject to limitations and assumptions both experimentally and numerically which may potentially affect the findings. Although the numerical model provides similar trends as the experimental measurements, there are still some discrepancies. Part of the explanation can come from the fact that the numerical model is perfectly axi-symmetric whereas the transducer used in the experiments may have some intrinsic defects which can result in asymmetry of the acoustic pressure even in the far field (Fig. 2a). Similar results have been reported in [16, 20, 23].

Both models assume that the cell culture medium is water. A review on the biologic materials used in the cell culture medium shows that their properties are very close to water properties [13]. Nonetheless, it would be interesting to investigate the influence of the introduction of the proper material with accurate properties to represent the cells and possible interactions of cells on the acoustic field inside the Petri dish.

There is also a lack of unanimity concerning the representative parameter of US stimulation. It should be reminded that although the I_{SATA} is a widely accepted parameter in research and development of the clinical devices, it seems that it may not be sufficient for the evaluation of the acoustic intensity due to the fact that the I_{SATA} calculation threshold ($25\% \times I_{SPTA}$ or -6 dB) is strongly dependent on I_{SPTA} where a typical extreme value can considerably change the computed I_{SATA}. Another example is the same I_{SATA} value which can be related to different I_{TA} distributions. In addition, the technical data sheet of the Exogen® indicates that it generates $I_{SATA} = 30$ mW/cm$^2 \pm 30\%$. This noticeable tolerance supports the argument that more rigorous criteria (*e.g.* descriptive statistics such as standard deviation and/or weighing methods)

alongside the I_{SPTA} and I_{SATA} should be applied to better describe the acoustic field. The influence of the heterogeneity of acoustic intensity on the cells inside the Petri dish should be studied in further work. Experimental improvements can be made to ensure that as many cells as possible are equally stimulated to optimize the interpretation of the biological response. The I_{TA} distribution is of prime interest in biological experiments as providing a uniform and optimal stimulation to the cells seeded inside a Petri dish is of a great concern.

5. Conclusion

US stimulation is believed to accelerate bone cell regeneration. Though in-vitro studies provide a better understanding of possible underlying mechanisms, it is still a challenge to measure the acoustic intensity delivered to cells. This study aimed to develop a numerical model mimicking the experimental set-up of in-vitro US stimulation incorporating an innovative absorbing system. This absorbing system is the prerequisite for monitoring the acoustic stimulation conditions and allowing the numerical model to predict the acoustic intensity level potentially delivered to the cells.

A wide variety of experimental protocols used for US stimulation makes it difficult to compare the results of existing literature. Therefore, the development of a numerical model in addition to a proven experimental device opens perspectives to estimate the acoustic intensity delivered to the cells inside a Petri dish under different configurations and acoustic parameters and thus take up the challenge of an optimized biological experimentation.

The developed set-up addresses biologists' concerns such as space and handling with an incubator and biocompatibility of the materials used to avoid contamination of the cell culture medium. In addition, the corresponding numerical model will help to keep all the process of the stimulation under full control which is not only a key factor for parametric studies, but also it can contribute to the interpretation of results obtained with commercial devices whose configurations and parameterization are imposed by the manufacturers.

Acknowledgment

This study is partially funded by the CNRS project AAP2017-OSEZ–BARON. The authors would like to thank Olivier Pot of the Laboratory of Mechanics and Acoustics (LMA). The authors also thank Wendy Silva and Lugdivine Leblond from Aix-Marseille University, and Ibrahim El Succar from Centrale Marseille for their internship work.

References

[1] J. D. Heckman, J. Mccabe, J. J. Rni, By non-invasive, low-intensity pulsed ultrasound, Journal of Bone and Joint Surgery 76 (1994) 26–34.

[2] P. Reher, E.-N. I. Elbeshir, W. Harvey, S. Meghji, M. Harris, The stimulation of bone formation in vitro by therapeutic ultrasound, Ultrasound in Medicine & Biology 23 (1997) 1251–1258.

[3] S. Angle, K. Sena, D. Sumner, A. Virdi, Osteogenic differentiation of rat bone marrow stromal cells by various intensities of low-intensity pulsed ultrasound, Ultrasonics 51 (2011) 281–288.

[4] Y. Azuma, M. Ito, Y. Harada, H. Takagi, T. Ohta, S. Jingushi, Low-intensity pulsed ultrasound accelerates rat femoral fracture healing by acting on the various cellular reactions in the fracture callus, Journal of Bone and Mineral Research 16 (2001) 671–680.

[5] C. W. Chan, L. Qin, K. M. Lee, W. H. Cheung, J. C. Y. Cheng, K. S. Leung, Dose-dependent effect of low-intensity pulsed ultrasound on callus formation during rapid distraction osteogenesis, Journal of Orthopaedic Research 24 (2006) 2072–2079.

[6] C. Rubin, M. Bolander, J. P. Ryaby, M. Hadjiargyrou, The use of low-intensity ultrasound to accelerate the healing of fractures, Journal of Bone and Joint Surgery 83 (2001) 259.

[7] E. Mayr, V. Frankel, A. Rüter, Ultrasound–an alternative healing method for nonunions?, Archives of Orthopaedic and Trauma Surgery 120 (2000) 1–8.

[8] F. Padilla, R. Puts, L. Vico, K. Raum, Stimulation of bone repair with ultrasound: a review of the possible mechanic effects, Ultrasonics 54 (2014) 1125–1145.

[9] J. W. Busse, M. Bhandari, T. A. Einhorn, E. Schemitsch, J. D. Heckman, P. Tornetta, K.-S. Leung, D. Heels-Ansdell, S. Makosso-Kallyth, G. J. e. a. Della Rocca, Re-evaluation of low intensity pulsed ultrasound in treatment of tibial fractures (trust): randomized clinical trial, BMJ Clinical Research 355 (2016) i5351.

[10] S. Schandelmaier, A. Kaushal, L. Lytvyn, D. Heels-Ansdell, R. A. Siemieniuk, T. Agoritsas, G. H. Guyatt, P. O. Vandvik, R. Couban, B. Mollon, et al., Low intensity pulsed ultrasound for bone healing: systematic review of randomized controlled trials, BMJ Clinical Research 356 (2017) j656.

[11] S. Mortazavi, S. Mortazavi, M. Paknahad, Mode & mechanism of low intensity pulsed ultrasound (LIPUS) in fracture repair, Ultrasonics 71 (2016) 142.

[12] P. Aspenberg, Is LIPUS the baby in the bathwater?, Acta Orthopaedica 88 (2017) 1.

[13] K. Hensel, M. P. Mienkina, G. Schmitz, Analysis of ultrasound fields in cell culture wells for in vitro ultrasound therapy experiments, Ultrasound in Medicine & Biology 37 (2011) 2105–2115.

[14] J. J. Leskinen, K. Hynynen, Study of factors affecting the magnitude and nature of ultrasound exposure with in vitro set-ups, Ultrasound in Medicine & Biology 38 (2012) 777–794.

[15] J. Crapps, A. Rahimi, N. Case, Analysis of a novel bioreactor designed for ultrasound stimulation of cell-seeded scaffolds, in: 2018 IEEE International

Symposium on Signal Processing and Information Technology (ISSPIT), IEEE, 2018, pp. 1–6.

[16] V. A. Khokhlova, S. M. Shmeleva, L. R. Gavrilov, E. Martin, N. Sadhoo, A. Shaw, Infrared mapping of ultrasound fields generated by medical transducers: Feasibility of determining absolute intensity levels, The Journal of the Acoustical Society of America 134 (2013) 1586–1597.

[17] A. Rahimi, N. Case, Computational model to evaluate modulation of the acoustic field in an ultrasonic bioreactor by incorporation of a water layer bounded by an acoustic absorbent boundary layer, Ultrasonics 103 (2020) 106086.

[18] D. A. Horne, P. D. Jones, M. S. Adams, J. C. Lotz, C. J. Diederich, LIPUS far-field exposimetry system for uniform stimulation of tissues in-vitro: development and validation with bovine intervertebral disc cells, Biomedical Physics & Engineering Express 6 (2020) 035033. Publisher: IOP Publishing.

[19] W. Secomski, K. Bilmin, T. Kujawska, A. Nowicki, P. Grieb, P. A. Lewin, In vitro ultrasound experiments: Standing wave and multiple reflections influence on the outcome, Ultrasonics 77 (2017) 203–213.

[20] M. Snehota, J. Vachutka, G. ter Haar, L. Dolezal, H. Kolarova, Therapeutic ultrasound experiments in vitro: Review of factors influencing outcomes and reproducibility, Ultrasonics 107 (2020) 106167.

[21] C.-H. Lai, S.-C. Chen, L.-H. Chiu, C.-B. Yang, Y.-H. Tsai, C. S. Zuo, W. H.-S. Chang, W.-F. Lai, Effects of low-intensity pulsed ultrasound, dexamethasone tgf-β1 and/or BMP-2 on the transcriptional expression of genes in human mesenchymal stem cells: chondrogenic vs. osteogenic differentiation, Ultrasound in Medicine & Biology 36 (2010) 1022–1033.

[22] J. G.-R. Li, W. H.-S. Chang, J. C.-A. Lin, J.-S. Sun, Optimum intensities

of ultrasound for pge2 secretion and growth of osteoblasts, Ultrasound in Medicine & Biology 28 (2002) 683–690.

[23] J. J. Leskinen, H. M. Karjalainen, A. Olkku, K. Hynynen, A. Mahonen, M. J. Lammi, Genome-wide microarray analysis of mg-63 osteoblastic cells exposed to ultrasound, Biorheology 45 (2008) 345–354.

[24] P. Acevedo, D. Das-Gupta, The measurement of the spatial average temporal average intensity isata and ultrasonic power w in composite ultrasonic transducers for medical application, Ultrasonics 40 (2002) 819–821.

[25] FDA, 501(k) guide for measuring and reporting acoustic output of diagnostic ultrasound medical devices, Food & Drug Administration (1985).

[26] R. C. Preston, Output measurements for medical ultrasound, Springer Science & Business Media, 1991.

[27] J. E. Mark, et al., Physical properties of polymers handbook, volume 1076, 2007.

[28] R. Courant, K. Friedrichs, H. Lewy, Über die partiellen differenzengleichungen der mathematischen physik, Mathematische Annalen 100 (1928) 32–74.

[29] J. Unsworth, S. Kaneez, S. Harris, J. Ridgway, S. Fenwick, D. Chenery, A. Harrison, Pulsed low intensity ultrasound enhances mineralisation in preosteoblast cells, Ultrasound in Medicine & Biology 33 (2007) 1468–1474.

[30] K. Bandow, Y. Nishikawa, T. Ohnishi, K. Kakimoto, K. Soejima, S. Iwabuchi, K. Kuroe, T. Matsuguchi, Low-intensity pulsed ultrasound (LIPUS) induces rankl, mcp-1, and mip-1β expression in osteoblasts through the angiotensin ii type 1 receptor, Journal of Cellular Physiology 211 (2007) 392–398.